ELSEVIER

International Journal of Mass Spectrometry 179/180 (1998) 67–76

International Journal of Mass Spectrometry

Production and magnetic analysis of beams of S atoms and SO radicals: a collisional study of their interactions with hydrogen molecules

Vincenzo Aquilanti[a,*], Daniela Ascenzi[a], Elisabetta Braca[b], David Cappelletti[b], Fernando Pirani[a]

[a]*Dipartimento di Chimica and* [b]*Istituto per le Tecnologie Chimiche, Università di Perugia I-06125, Perugia, Italy*

Received 16 March 1998; accepted 11 May 1998

Abstract

An intense and stable continuous beam of S atoms and SO radicals has been produced with a microwave discharge source operating in the Torr range in mixtures of SO_2 with various gases. The beam emerging from the plasma source was velocity analyzed by a mechanical velocity selector and detected by a quadrupole mass filter. Stern-Gerlach magnetic analysis indicates that both species are mainly generated in their electronic ground state and in the case of sulfur atoms with fine-structure levels, populated according to their degeneracies. Total integral cross section measurements are reported, as a function of velocity in the range 1.0–2.5 km $\times$ s^{-1}, for the scattering of $S(^3P_J)$ atoms and SO ($^3\Sigma$) radicals by D_2 molecules. The analysis of experimental data (cross sections and their velocity dependence, which exhibits glory interference patterns) allows a characterization of the spherically average component of the interaction potential for the investigated systems. A discussion of the effect of the Σ-Π splitting, spin-orbit, and electrostatic (including quadrupole–quadrupole) interaction on the dependence of the hydrogen molecule orientation is given for the S–H_2 potential energy surface. (Int J Mass Spectrom 179/180 (1998) 67–76) © 1998 Elsevier Science B.V.

Keywords: S; SO beams; Magnetic analysis; Collisional study; Interaction with H_2

1. Introduction

Scattering experiments with molecular beams at high angular and energy resolutions and with control of internal states are one of the most important sources of information on van der Waals intermolecular forces. The current focus on open shell species, such as atoms or radicals, is motivated by the need to describe inelastic processes concerning both fine structure transitions in collisions of open shell atoms with spherical partners [1] and fine structure and/or rotational excitations in collisons between open shell atoms and molecules [2], to characterize the role of the long range forces and the effect of the spin-orbit interaction in the selectivity of chemical reactions [3], to understand nature and properties of such weak forces that exhibit an intermediate behavior between chemical bonds and van der Waals interactions [4], to interpret by realistic potential energy functions the dynamics of photodissociation in clusters and solid matrices [5], and finally, to accurately describe transport properties of open shell atoms in inert gas baths [6].

Collisional experiments with unstable species re-

* Corresponding author.

Dedicated to Professor Fulvio Cacace in recognition of his outstanding contributions for many decades to gas-phase ion chemistry and physics.

PII S1387-3806(98)14050-2

quire extension and improvement of molecular beam techniques, with special care devoted to the production, detection, and characterization of intense beams of the desired species.

Microwave and radiofrequency discharge plasmas are often used as sources of near effusive and supersonic beams, respectively: atoms, free radicals, and molecules, produced in such conditions from dissociation of the precursor molecules in the plasma, are typically generated in a distribution of quantum states, whose relative population is further affected by collisional quenching with the source chamber walls and with other species. Therefore, in a molecular beam apparatus, both velocity selection and state analysis are crucial to completely separate the relative contributions of each species to the beam intensity, and to characterize and control the distribution of the internal states. By exploiting the selective deflection in an inhomogeneous magnetic field of velocity selected species for which the paramagnetism differs for different internal quantum states, the magnetic substrates distribution of atoms such as O [7], N [8], F [9,10], and Cl [11] in effusive beams was analyzed and the role of excited states assessed.

The same approach has been recently applied [12] to analyze supersonic beams of N, O, and Cl atoms employed in parallel experiments of reactive scattering [13].

Total integral scattering cross section measurements, as a function of beam velocity, have previously been performed by using magnetically selected thermal effusive beams of $O(^3P_J)$ [7,14], $F(^2P_J)$ [9,10], and $Cl(^2P_J)$ [3,15,16] atoms as projectiles and rare gases or simple molecules (D_2, CH_4) as targets. These experiments provided an accurate characterization of potential curves correlating at a large intermolecular distance R with specific atomic sublevels. Although most of these atom–molecule pairs can also lead to reaction, with activation energies varying between few and several kcal/mol, the collision energies are typically so low that the analysis of total integral scattering cross section results provided information on the interaction in the entrance valleys to the manifold of potential energy surfaces that correlate reactants in the electronic ground state to products in different quantum states. In particular, the effect of the spin-orbit coupling on the interaction has been defined and the role of the electronic anisotropy discussed.

For the F–H_2 system the obtained interaction has subsequently been taken as a starting point to interpret reactive [17] and rotationally inelastic [18] scattering results. In the latter study, a dependence of the long range part of the potential energy surfaces on the hydrogen molecule orientation has been proposed.

The purpose of the present work was to determine, through scattering studies, the interaction features for the S–H_2 and SO–H_2 systems. The interest in these systems arises from the important role played by S atoms and SO radicals in a variety of processes occurring in interstellar molecular clouds, in the combustion of fuels rich in sulfur species (such as H_2S), and in reactions responsible for air pollution. Furthermore, although $S(^3P)$ and $O(^3P)$ atoms belong to the same group, their reactions with hydrogen molecules differ markedly with respect to endothermicity and activation energy:

$$O(^3P) + H_2 \rightarrow OH + H \quad \Delta H_0^0 = 1.96 \text{ kJ mol}^{-1} \text{ [19]}$$

$$E_a \simeq 26 \text{ kJ mol}^{-1} \text{ [19]}$$

$$S(^3P) + H_2 \rightarrow SH + H \quad \Delta H_0^0 = 82.8 \text{ kJ mol}^{-1} \text{ [20]}$$

$$E_a \simeq 83 \text{ kJ mol}^{-1} \text{ [21,22]}$$

That the activation energy of the sulfur atom reaction is very close to the endothermicity indicates a small barrier for the reverse reaction, in contrast to oxygen, for which the barrier is substantial.

For both reactions the intermediate and long range behavior of the potential energy surfaces in the entrance channel for the forward direction are controlled by interactions of the same nature, such as induced multipole–induced multipole attraction and an electrostatic contribution plus specifically chemical (essentially charge transfer) and spin-orbit effects.

In Sec. 2 we present a brief description of the experimental apparatus used for the production, characterization, and scattering of effusive beams of S

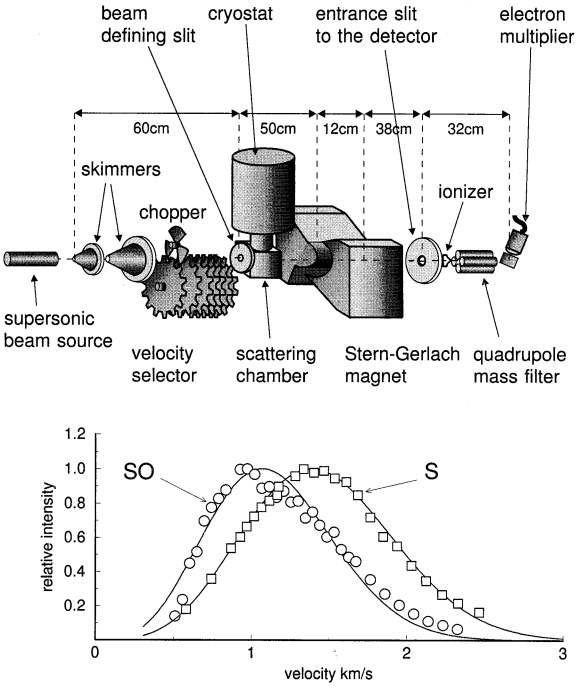

Fig. 1. Experimental apparatus for beam production, velocity, and internal state analysis and total integral scattering cross section measurements. The lower panel shows velocity distributions of SO and S species produced in the microwave discharge; best-fit calculations assuming Boltzmann distributions are reported as solid lines.

atoms and SO radicals. In Sec. 3 the magnetic analysis of internal states is discussed, and total integral scattering cross sections are presented in Sec. 4. A discussion and conclusions follow in Secs. 5 and 6.

2. Experimental setup

The present experimental apparatus, presented in Fig. 1, is basically the same as previously used in the magnetic analysis and scattering experiments with other open shell species [3,7–11,14–16], and therefore only some general features and those details specifically relevant for the production, characterization, detection, and scattering of beams of S atoms and SO radicals will be outlined in the following text.

The apparatus consists of a set of differentially pumped vacuum chambers where the beam, produced in the discharge source, is mechanically velocity selected [to within 5% full width at half maximum (fwhm)] by a series of rapidly spinning slotted disks and is subsequently analyzed by a Stern-Gerlach magnet in Rabi configuration [23] whose use will be detailed in Sec. 3. Detection is by electron bombardment ionization and quadrupole mass spectrometry. The detector housing is maintained under ultra-high vacuum conditions ($\sim 10^{-10}$ Torr).

The beam source consists of a quartz cell confined inside a near-resonant microwave cavity operating at 2450 MHz and a nominal power of ~100 W. Several attempts have been made to produce S atoms and SO radicals [24] by electric discharge in SO_2, both pure and in mixtures with various gases (Ar, N_2, O_2, and He). Mass spectrometric analysis has revealed the presence in such beams of species of higher masses produced in the plasma. Optimal yield (i.e. beam intensity sufficiently high in a wide velocity range) and minimal interference from parent ion fragmentation in the mass spectrum at the mass-to-charge ratio $m/z = 48$ and $m/z = 32$ have been obtained with a microwave plasma generated in a 1:1 He:SO_2 gaseous mixture at a total pressure of ~4 Torr. Molecular beam analysis has also clarified the nature of the signal measured at $m/z = 32$, because the detection of sulfur atoms can be contaminated by the presence of molecular oxygen, which might be formed in the discharge and detected at the same m/z ratio. In order to determine how much of the signal derives from sulfur atoms, we have simultaneously measured peak intensities in the mass spectrum at both $m/z = 32$ and 34, the latter due to the isotope ^{34}S and to isotopic $^{16}O^{18}O$ molecular oxygen. According to natural isotopic percent abundances (95.02% for ^{32}S and 4.21% for ^{34}S; 99.76% for ^{16}O and 0.20% for ^{18}O) it should detect a signal ratio $m_{34}/m_{32} = 0.002$ if the beam is exclusively formed by O_2 molecules, and the signal ratio should increase to 0.044 in the case of the exclusive presence of sulfur atoms. The measured ratio $\simeq 0.04$ is a clear evidence that the latter case applies. A further control on the composition of the beam, performed by the coupling of magnetic analysis with velocity selection, will be discussed in Sec. 3.

Under typical operative conditions the extent of dissociation of the SO_2 precursor in the source is

estimated from relative beam intensities to be about 50%. Velocity distributions of S atoms and SO radicals (Fig. 1) formed in an approximately 2:1 ratio are sufficiently broad to enable magnetic analysis and scattering experiments to be performed in a wide velocity range. Because the higher mass species present in the beam originate a large contribution from fragmentation in the lower tail of the velocity spectrum of both $m/z = 32$ and 48, all the experiments were performed at beam velocities sufficiently high ($v \geq 1.0$ km s^{-1}) to prevent such a contamination (Fig. 1).

In the third chamber, after a path of ~60 cm from the source, and before the entrance to the magnetic selector, the beams undergo a final collimation by a defining slit of 0.35 mm in radius, and then they cross a copper chamber where the pressure is increased from 10^{-6} to ~10^{-3} Torr by adding the target gas for measurements of the beam attenuation due to scattering. The chamber is cooled at solid air temperature (~70 K) in order to decrease the blurring of quantum interference effects by the thermal motion of the target gas. In the present experiments, the use of D_2 instead of H_2 as the target gas is crucial to a further reduction of the collision energy spread. As usual absolute values for total integral cross section data as a function of the beam velocity have been obtained from beam attenuation measurements and using an internal calibration procedure [25].

The distance from the scattering chamber to the detector is long enough, when compared with the sufficiently narrow beam emerging from the defining slit before the scattering chamber, that, for the present scattering experiments, no correction is necessary to account for the finite angular resolution of the apparatus [26].

3. Molecular beam characterization by magnetic analysis

As we have seen, in the present experiments S atoms and SO radicals are produced from a microwave discharge source, therefore it appears useful to assess the role of possible metastable electronic states that could be formed in the discharge plasma. Indeed for the SO radical, as in the similar case of the O_2 molecule [23,27], not only the ground $^3\Sigma^-$ but also the excited and long lived metastable $^1\Delta$ and $^1\Sigma^+$ states, which lie respectively ~6350 cm^{-1} (0.787 eV) and 10510 cm^{-1} (1.30 eV) [28] above the ground $^3\Sigma^-$ level, can be expected to be populated in the plasma. Their lifetimes, ~450 ms [29] and ~6 ms [30], respectively, are sufficiently long for them to survive during the flight time in the apparatus (<1 ms).

As far as S atoms are concerned, the first electronic excited state $^1D_2$ lies 1.14 eV [31] over the ground ^3P state and its lifetime is so long (~28 s [32]) that all metastable atoms produced in the source reach the detector.

As before [3,7–11,14–16,24], the characterization of beams containing open shell species is performed in the transmission mode with a Stern-Gerlach magnetic selector inserted along the beam path and collocated, in the present experiments, at a distance of 110 cm from the nozzle source (Fig. 1). The beam transmittance (i.e. the ratio I/I_0 between the beam intensity with and without the magnetic field) is measured as a function of the applied field B at a selected beam velocity v. The action of an inhomogeneous magnetic field on a beam composed of paramagnetic species of the same mass and velocity is to induce different deflections depending on the values of the effective magnetic moments of the various particles. For a species in a defined quantum state i, to which a potential energy $E_i(B)$ is associated as a function of the field strength B, the effective magnetic moment μ_i is given by

$$\mu_i = -\frac{\partial E_i}{\partial B}$$

Accordingly, the measured beam transmittance, which is determined by μ_i, strongly depends on the features and distribution of quantum states. An important problem to be solved, before planning magnetic analysis experiments of any type, concerns the determination of the dependence of E_i (or μ_i) on B, related to the change as a function of B in the angular momentum coupling scheme followed by the particle in the i state. The sulfur atom has a nuclear spin equal

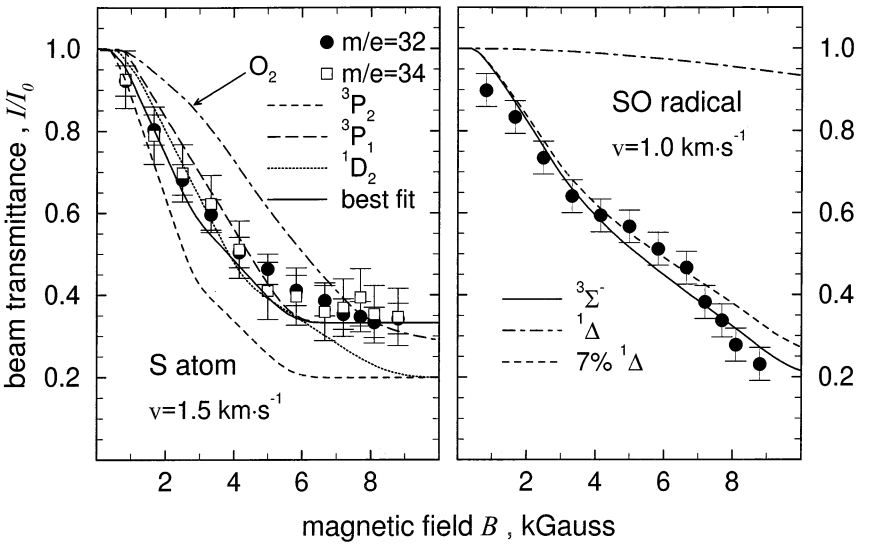

Fig. 2. Beam transmittances I/I_0 as a function of the magnetic field intensity B for S atoms and SO radicals at selected beam velocities v. Results of calculations assuming each species in a defined electronic state are also shown for comparison. In the S atom panel the dotted-dashed curve is calculated assuming that the signal at $m/z = 32$ is due to O_2 molecules in a mixture of ground $^3\Sigma_g^-$ and excited $^1\Delta_g$ electronic states in the ratio 9:1 [27]. Best fit is obtained assuming a "statistical" population ratio of J levels for the ground ^{3}P state, $^3P_2$:$^3P_1$:$^3P_0$ = 5:3:1. In the SO radical panel the dashed curve is calculated assuming that 7% of the molecules are in the excited $^1\Delta$ state and that the rotational temperature T is 1500 K, as estimated in Aquilanti et al. [24].

to zero on both its isotopic components ^{32}S and ^{34}S and exhibits a strong coupling between orbital $\boldsymbol{L}$ and spin $\boldsymbol{S}$ angular momenta to give the total electronic angular momentum $\boldsymbol{J}$. The energy splitting $\Delta_{J,J+1}$ between fine levels in the ^3P_J ground electronic state, $\Delta_{1,2}$ = 49.12 meV and $\Delta_{0,2}$ = 71.09 meV [31], are sufficiently high that any decoupling of $\boldsymbol{J}$ in $\boldsymbol{L}$ and $\boldsymbol{S}$ (Paschen-Back effect) can be neglected at the magnetic field strengths used in our apparatus (≤10 kGauss). Accordingly, for both ^3P_J and $^1D_2$ states, μ_i can be calculated [23] by the equation

$$\mu_{J_{m_J}} = \mu_0 g_J m_J$$

where μ_0 is the Bohr magneton, m_J is the $\boldsymbol{J}$ component along $\boldsymbol{B}$ and the Landè factor g_J, relative to the quantum number J, is equal to 1.5 for all J fine levels of the ^{3}P state, and to 1.0 in the metastable $^1D_2$ level.

The situation for the SO radical is complicated by the coupling of spin and electronic orbital angular momenta with the rotational motion and by its partial decoupling in the magnetic field (see Aquilanti et al. [24]). In such a case the $\mu_i(B)$ values for $^3\Sigma^-$ and $^1\Delta$ states are obtained as described in Aquilanti et al. [24], and the $^1\Sigma^+$ metastable level is expected to be fully diamagnetic.

The transmittance I/I_0 has been measured as a function of the applied magnetic field B at different velocities for both S and SO beams and typical results are reported in Fig. 2. In the case of S atoms at v = 1.5 km × s^{-1}, experiments have been performed using both m/z = 32 and 34 mass spectrometric signals: measured beam transmittance data (see left panel of Fig. 2) are indistinguishable within the error bars, representing a confirmation that signals at both masses are mainly due to sulfur atoms. As a further comparison, the transmittance calculated at the same velocity for an O_2 molecular beam is also reported in Fig. 2 (dotted-dashed line in the left panel) and clearly shows a completely different behavior.

Also in Fig. 2, experimental data are compared with calculations that assume that the S and SO beams are exclusively formed by particles in a defined electronic state i. The comparison suggests that the produced beam is mainly formed by S atoms and SO

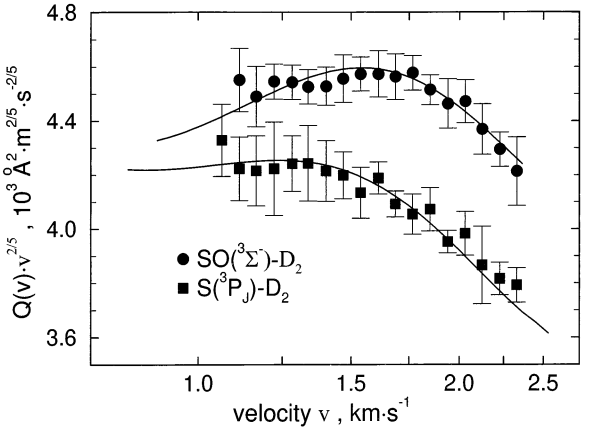

Fig. 3. Total integral cross section $Q(v)$ for the S–D_2 and SO–D_2 systems as a function of the beam velocity v. Full lines are calculated assuming a spherical potential interaction $V_0(R)$ (see Fig. 4).

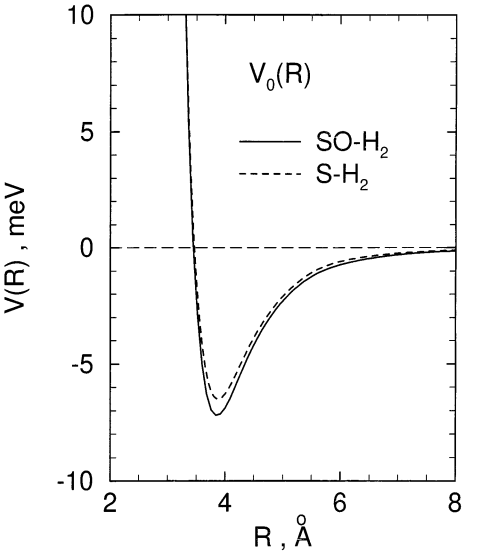

Fig. 4. Interaction potentials $V_0(R)$, for the S–H_2 and SO–H_2 systems.

radicals in their electronic ground states, the concentration of metastable species not exceeding a few percent. Present results are also in agreement with previous determinations on effusive molecular O_2 [27] and atomic oxygen beams [3,8,9]. In addition fine levels J of the ^3P_J ground state of S atoms are found to be typically populated in their statistical ratio, $^3P_2$:$^3P_1$:$^3P_0$ = 5:3:1.

4. Total integral cross section measurements: data analysis and interaction potentials

The absolute values of total cross section $Q(v)$, for the scattering of S and SO species by D_2 molecules, measured as a function of the beam velocity v, are reported in Fig. 3 where they are plotted as $Q(v) \times v^{2/5}$ to emphasize undulations due to the "glory" interference effect. It has long been established [33] that glory undulations are semiclassically attributed to the interference between two types of trajectories, both leading to a zero deflection angle; the first type corresponding to trajectories at intermediate impact parameters, for which the attractive and repulsive actions balance, and the second type to collisions at impact parameters so large that the effect of the potential is negligible. Amplitudes and frequencies of glory undulations are therefore related to features of the potential in the intermediate intermolecular distance range and are a probe of the well depth ϵ and its location R_m. The monotonic component of $Q(v)$, which decreases as $v^{-2/5}$ is mainly responsible for the size of the cross section, being determined by collisions at large impact parameters (which lead to small deflection angles). This component is a probe of the long range part of the interaction [34].

An analysis of the scattering data for both systems has been attempted by neglecting any interaction anisotropy effect and describing the interactions in terms of spherical potential models (i.e. only dependent on the intermolecular distance R). As usual, we employ an MSV (Morse-spline-van der Waals, see Aquilanti et al. [3,24]) parameterization for the interaction and standard computational techniques [35] for cross section calculations. Calculated cross sections are compared with those experimentally measured in Fig. 3, where they are plotted as solid lines, and the best fit potentials are shown in Fig. 4. From scattering data analysis a long range effective dipole–dipole constant C_0, which includes contributions from higher order terms, as well as the well depth ϵ and its location R_m, are obtained. They are reported in Table

Table 1
Potential parameters of the spherical $V_0(R)$ component for $S(^3P_J)$ and $SO(^3\Sigma^-)$ interacting with hydrogen molecules. The estimated errors are ~15% for the well depth ϵ and long range constant C_0 and ~3% for the well location R_m (in parentheses are values obtained from correlation formulas [36]).

	$S(^3P_J)$	$SO(^3\Sigma^-)$
R_m (Å)	3.88 *(3.84)*	3.86 *(3.92)*
ϵ (meV)	6.5 *(6.4)*	7.2 *(7.2)*
C_0 (meV Å^6)	2.8×10^4 *(2.85×10^4)*	3.5×10^4 *(3.61×10^4)*

1, together with estimated uncertainties, and are compared with results anticipated from previously proposed empirical formulas [36], which correlate the potential parameters to the polarizabilities of the interacting partners. Because these formulas were originally formulated only for typical van der Waals interactions, the agreement between experimental results and predictions indicates that, for present systems, total cross sections yield information on the average component of the interactions, whose intermediate and long range behavior is dominated by van der Waals forces.

5. Discussion

The success of the present analysis in reproducing total integral cross sections and their collision velocity dependence suggests that, under present experimental conditions, an essentially isotropic interaction drives the collisions in both S–D_2 and SO–D_2 systems and that anisotropy effects due to the open shell nature of the S atom, and to different molecular orientations of the SO radical and D_2 molecule, play only a minor role.

In the SO–D_2 system the main contribution to the anisotropy is of the van der Waals type and can be related to the variation of the molecular size and of the induced multipole interaction as the two partners change their relative orientation.

This isotropic behavior of the SO radical and of the D_2 molecule in the SO–D_2 collisional complex stems from the fact that the rotational temperature of SO in the beam (~1500 K [24]) and of deuterium molecules in the scattering chamber (~70 K) are sufficiently high to induce, at the low kinetic energies of the present experiments, an appreciable averaging of the anisotropic interaction probed during the collision time. Also, in such a situation rotationally inelastic transitions are less effective and the system behaves adiabatically with respect to the vibrations of both partners. It should also be noted that even though the use of the heavier D_2 instead of H_2 and the cooling of the scattering chamber at solid air temperature allow us to resolve the glory pattern by reducing the effect of the thermal motion of the target molecules, such an effect is still sufficiently high to mask the small glory quenching associated to anisotropic effects.

In the S–D_2 system there are two additional sources of anisotropy to be considered besides the contribution due to van der Waals forces. As before the strength of this van der Waals component (extensively studied for example for the Ne–D_2 and Ar–D_2 systems through rotational inelastic scattering experiments [37,38]) is expected to amount to only a few percent of the isotropic interaction: as in previous experiments [3,10,14], the effect of this component is cancelled by averaging over rotational and translational motions of D_2 molecules.

A further contribution to the anisotropy of the interaction is operative in those systems involving open shell atoms with high electron affinity A. Previous scattering studies of $Cl(^2P_J$, $A = 3.6$ eV) [3,15,16], $F(^2P_J$, $A = 3.4$ eV) [9,10], and $O(^3P_J$, $A = 1.5$ eV) [7,14] by closed shell partners led us to interpret this component as a configuration interaction between the neutral ground and the ionic excited potential surfaces of the same symmetry, thus introducing a partial "chemical" contribution to the bond. The strength of this interaction component depends on the difference between the ionization potential (I) of the closed shell partner and the electron affinity A of the open shell atom. Its anisotropy arises by the change in charge transfer effects that take place when the orientation of the half filled orbitals of the open shell atom, relative to the other partner, is varied. This interaction contribution is expected to be of some relevance for the system under study because the

electron affinity of $S(^3P_J)$ is sufficiently high (A = 2.07 eV).

Indeed, in a parallel scattering experiment involving S–Ne, Ar, and Kr systems [39], we have observed a quenching of the glory structure, whose amount increases in going from Ne to Kr along with the decrease of the ionization potential of rare gas atoms. A quantitative analysis of the experimental data has been performed in terms of an adiabatic scheme where the collision of a ^3P_J open shell atom with a closed shell particle is considered as evolving along six effective adiabatic potential curves $V_{J\Omega}(R)$, where Ω is the absolute value of the projection of J along R, each one correlating at large intermolecular distances R, with a defined $|J\ m_J\rangle$ atomic sublevel. As before [7,40] the adiabatic potentials are given in terms of an average spherical interaction, an anisotropic component, and the spin orbit constants of the open shell atom. As in previously studied cases of $O(^3P)$ [7,14], $F(^2P)$ [9,10], and $Cl(^2P)$ [3,15,16], it has been found for $S(^3P)$ that the potential parameters of the spherical interaction are consistent with those of typical van der Waals interactions, whereas the strength of the anisotropic component is as expected for the configuration interaction due to a single electron exchange [4]. Accordingly the correlation formula from Aquilanti et al. [4], given in terms of the energy separation between the two coupled states and the well depth of the isotropic component, can be used here to predict the strength of the electronic anisotropy for the interaction between $S(^3P_J)$ and hydrogen molecules. The anisotropic term has been represented as previously (see Aquilanti et al. [3] for example) with an (exp,6) Buckingham-type model with the strength preexponential parameter A_2 = 345 eV estimated from the correlation formula and the long range constant fixed by the polarizability anisotropy of S atoms [39]. The R dependence has been assumed to be the same as for the S-rare gas systems [39]. This prediction, and the potential parameters obtained in the previous section, can be used to generate the electrostatic interactions V_Σ and V_Π for the $S(^3P_J)$-molecular hydrogen system, where the molecule is considered to be a structureless particle (Fig. 5). The symbols Σ and Π stand for Λ = 0 and 1, respectively,

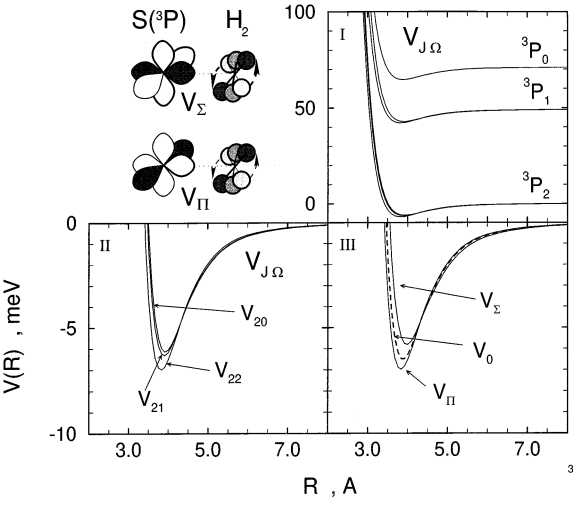

Fig. 5. Potential energy curves for the $S(^3P_J)$–H_2 system: (I) $V_{J\Omega}$ adiabatic potential energy curves correlating at long range with the atomic fine structure levels ^3P_J; (II) blow up of the ground $V_{2\Omega}$ states; (III) the electrostatic interactions V_Σ and V_Π and their "average" $V_0 = (V_\Sigma + 2V_\Pi)/3$.

where the quantum number Λ, the absolute value of the projection of the electronic orbital angular momentum $\boldsymbol{L}$ along $\boldsymbol{R}$, indirectly defines allowed orbital orientations of the open shell atom within the complex. V_Σ and V_Π interactions, together with the fine structure level separations of the $S(^3P_J)$ atom, can be used to build up the effective adiabatic potential curves $V_{J\Omega}(R)$ reported in Fig. 5. The comparison between pure V_Σ and V_Π electrostatic interactions and the effective adiabatic curves shows the important role played in this system by the spin orbit coupling in reducing the interaction anisotropy through the mixing of the Σ and Π characters. A test of the present analysis is obtained by calculating individual total cross sections $Q_{J\Omega}$ for scattering by the six adiabatic potential curves $V_{J\Omega}(R)$, and combining them according to the weights of $S(^3P_J)$ levels determined as in Sec. 3. Results convoluted in the laboratory reference frame are indistinguishable, within the linewidth in Fig. 3, from previous ones, where only the spherical component of the interaction was considered. An upper experimental limit to the V_Σ–V_Π splitting can be estimated by increasing the strength of the anisotropy further to produce an appreciable quenching of

the glory amplitude. This upper limit has been found to be approximately a factor of two higher than the value obtained from the correlation formula.

A third and final contribution to the anisotropy is of electrostatic nature and originates from the permanent quadrupole–permanent quadrupole interaction. The effect of this anisotropic contribution is strongly attenuated by the rotation of the hydrogen molecule during the collision, but an evaluation of its strength is of general interest for many other applications.

The quadrupole moment for an S atom can be predicted from the mean square radius of its $3p$ orbital [32] as $5.12\ e \times a_0^2$, whereas a value of $0.48\ e \times a_0^2$ for hydrogen molecules is given in Stogryn and Stogryn [41]. The effect of the quadrupole–quadrupole interaction, which has an R^{-5} dependence, varies with the orientation of the hydrogen molecule with respect to the orbital configuration of the S atom and therefore its effect depends also on the electronic symmetry of the potential energy surface. Potential curves in Fig. 6 describe the orientational dependence of the electrostatic interaction in a diabatic representation (for a similar approach to an analogues case, see Dubernet and Hutson [42]). As can be seen, the quadrupole–quadrupole interaction produces a stabilization of the state of Σ symmetry and a destabilization of the states of Π symmetry for the collinear $C_{\infty v}$ configuration. An opposite behavior shows up with the C_{2v} configurations. These interaction potentials can be used, properly introducing spin-orbit coupling, to assess asymptotic behavior of the manifold of anisotropic potential energy surfaces for this reactive system.

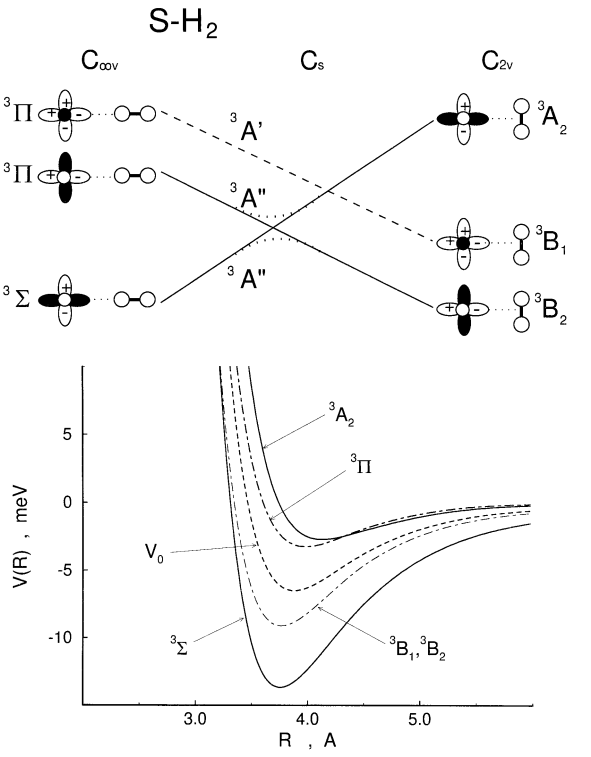

Fig. 6. Cuts of the potential energy surfaces for the $S(^3P_J)$–H_2 system are reported in the lower panel for the two limiting $C_{\infty v}$ and C_{2v} configurations, together with the spherically averaged interaction term $V_0(R)$. In the upper panel the correlation diagram is given among electronic states as the angle between the molecular axis and the direction of approach is varied between collinear ($C_{\infty v}$) and perpendicular (C_{2v}) configurations (filled orbitals are in black, signs of wavefunctions for those occupied by a single electron are indicated). For nonlinear C_s geometries, the components of the same symmetry are mixed giving an adiabatically avoided crossing.

Acknowledgements

This work is supported by the Italian National Research Council (CNR), by the Ministero dell'Università e della Ricerca Scientifica e Tecnologica (MURST), and by the European Union within the Training and Mobility of Researchers Network "Potential Energy Surfaces for Molecular Spectroscopy and Dynamics" (contract no. ERB-FMRX-CT96-0088).

References

[1] (a) I.S. Fletcher, D. Husain, 49 (1977) 516; (b) V. Aquilanti, G. Grossi, A. Laganà, Nuovo Cimento 363 (1981) 7; (c) A.I. Chichinin, L.N. Krasnoperov, Chem. Phys. Lett. 160 (1989) 448; (d) G.S. Tyndall, J.J. Orlando, C.S. Kegley-Owen, J. Chem. Soc. Faraday Trans. 91 (1995) 3055.
[2] (a) Z. Ma, K. Liu, Chem. Phys. Lett. 213 (1993) 269; (b) M. Faubel, L.Y. Rusin, S. Schlemmer, F. Sondermann, U. Tappe, J.P. Toennies, J. Chem. Soc. Faraday Trans. 89 (1993) 1475.
[3] V. Aquilanti, D. Cappelletti, F. Pirani J. Chem. Soc. Faraday Trans. 89 (1993) 1467.
[4] V. Aquilanti, D. Cappelletti, F. Pirani Chem. Phys. Lett. 271 (1997) 216.
[5] (a) J.G. McCaffrey, H. Kunz, N. Schwentner, J. Chem. Phys. 96 (1992) 155; (b) A. Garcia-Vela, R.B. Gerber, J.J. Valentini,

J. Chem. Phys. 97 (1992) 3297; (c) W.G. Lawrence, V.A. Apkarian, J. Chem. Phys. 97 (1992) 2229; (d) W.G. Lawrence, V.A. Apkarian, J. Chem. Phys. 101 (1994) 1820; A.I. Krylov, R.B. Gerber, R.D. Coalson, J. Chem. Phys. 105 (1996) 4626;
[6] V. Aquilanti, F. Vecchiocattivi, Chem. Phys. Lett. 156 (1989) 109.
[7] V. Aquilanti, R. Candori, F. Pirani, J. Chem. Phys. 89 (1988) 6157.
[8] B. Brunetti, G. Liuti, F. Pirani, E. Luzzatti, Chem. Phys. Lett. 84 (1981) 201.
[9] V. Aquilanti, E. Luzzatti, F. Pirani, G.G. Volpi, J. Chem. Phys. 89 (1988) 6165.
[10] V. Aquilanti, R. Candori, D. Cappelletti, E. Luzzatti, F. Pirani, Chem. Phys. 145 (1990) 293.
[11] V. Aquilanti, R. Candori, D. Cappelletti, V. Lorent, F. Pirani, Chem. Phys. Lett. 192 (1992) 145.
[12] M. Alagia, V. Aquilanti, D. Ascenzi, N. Balucani, D. Cappelletti, L. Cartechini, P. Casavecchia, F. Pirani, G. Sanchini, G.G. Volpi, Israel J. Chem. 37 (1997) 329.
[13] (a) M. Alagia, N. Balucani, P. Casavecchia, D. Stranges, G.G. Volpi, J. Chem. Soc. Faraday Trans. 91 (1995) 575; (b) M. Alagia, N. Balucani, L. Cartechini, P. Casavecchia, E.H. van Kleef, G.G. Volpi, F.J. Aoiz, L. Banares, D.W. Schwenke, T.C. Allison, S.L. Mielke, D.G. Truhlar, Science 273 (1996) 1519.
[14] V. Aquilanti, R. Candori, L. Mariani, F. Pirani, G. Liuti, J. Phys. Chem. 93 (1989) 130.
[15] V. Aquilanti, D. Cappelletti, V. Lorent, E. Luzzatti, F. Pirani, Chem. Phys. Lett. 192 (1992) 153.
[16] V. Aquilanti, D. Cappelletti, V. Lorent, F. Pirani, J. Phys. Chem. 97 (1993) 2063.
[17] (a) G.D. Billing, L. Yu. Rusin, M. Sevryuk, J. Chem. Phys. 103 (1995) 2482; (b) V. Aquilanti, S. Cavalli, D. De Fazio, A. Volpi, A. Aguilar, X. Gimenez, J.M. Lucas, J. Chem. Phys., in press.
[18] F.A. Gianturco, F. Ragnetti, M. Faubel, B. Martinez-Háya, L.Y. Rusin, F. Sondermann, U. Tappe, Chem. Phys. 200 (1995) 405.
[19] D.L. Baulch, C.J. Cobos, R.A. Cox, C. Esser, P. Frank, T. Just, J.A. Kerr, M.J. Pilling, J. Troe, R.W. Walker, J. Warnatz, J. Phys. Chem. Ref. Data 21 (1992) 411.
[20] M.W. Chase Jr., C.A. Davies, J.R. Downey Jr., D.J. Fruip, R.A. McDonald, A.N. Syverud, JANAF Thermochemical Tables, J. Phys. Chem. Ref. Data 14 (1985) (suppl 1), 1896.
[21] H. Shiina, M. Oya, K. Yamashita, A. Miyoshi, H. Matsui J. Phys. Chem. 100 (1996) 2136.
[22] D. Woiki, P. Roth, Int. J. Chem. Kinet. 27 (1995) 547.
[23] V. Aquilanti, D. Ascenzi, D. Cappelletti, F. Pirani, J. Chin. Chem. Soc. 42 (1995) 263.
[24] V. Aquilanti, D. Ascenzi, E. Braca, D. Cappelletti, G. Liuti, E. Luzzatti, F. Pirani, J. Phys. Chem. A 101 (1997) 6523.
[25] V. Aquilanti, G. Liuti, F. Pirani, F. Vecchiocattivi, G.G. Volpi, J. Chem. Phys. 65 (1976) 4751.
[26] (a) P. Kusch, J. Chem. Phys. 40 (1964) 1; (b) F. von Busch, Z. Physik 193 (1966) 412; (c) H. Pauly, J.P. Toennies, in Methods of Experimental Physics A, Vol. 7, Academic, San Diego, 1968 p. 227; (d) P. Dehmer, L. Wharton, J. Chem. Phys. 57 (1972) 4821; (e) J.J.H. van de Biesen, in G. Scoles (Ed.), Atomic and Molecular Beam Methods, Oxford University, Oxford, 1988.
[27] V. Aquilanti, D. Ascenzi, D. Cappelletti, F. Pirani, Int. J. Mass Spectrom. 149/150 (1995) 355.
[28] W.W. Clark, F.C. De Lucia, J. Mol. Spectr. 60 (1976) 332.
[29] R. Klotz, C.M. Marian, S.D. Peyerimhoff, B.A. Hess, R.J. Buenker, Chem. Phys. 223 (1984) 223.
[30] J. Wildt, E.H. Fink, R. Winter, F. Zabel, Chem. Phys. 80 (1983) 167.
[31] C.E. Moore, Atomic Energy Levels, Vol. 1, National Bureau of Standards, Washington, DC (1949).
[32] A.A. Radzig, B.M. Smirnov, Reference Data on Atoms, Molecules and Ions, Springer-Verlag, Berlin, 1985.
[33] (a) R.B. Bernstein, T.J.P. O'Brien, Discuss. Faraday Soc. 40 (1965) 35; (b) R.B. Bernstein, T.J.P. O'Brien, J. Chem. Phys. 46 (1967) 1208.
[34] (a) R.B. Bernstein, K.H. Kramer, J. Chem. Phys. 38 (1963) 2507; (b) G.B. Ury, L. Wharton, J. Chem. Phys. 50 (1972) 5832.
[35] F. Pirani, F. Vecchiocattivi, Mol. Phys. 45 (1982) 1003.
[36] (a) R. Cambi, D. Cappelletti, G. Liuti, F. Pirani, J. Chem. Phys. 95 (1991) 1852; (b) D. Cappelletti, G. Liuti, F. Pirani, Chem. Phys. Lett. 183 (1991) 297.
[37] J. Andres, U. Buck, F. Huisken, J. Schleusener, F. Torello, J. Chem. Phys. 73 (1980) 5621.
[38] U. Buck, Faraday Disc. Chem. Soc. 73 (1982) 187.
[39] V. Aquilanti, D. Ascenzi, E. Braca, D. Cappelletti, F. Pirani, unpublished.
[40] V. Aquilanti, G. Liuti, F. Pirani, F. Vecchiocattivi, J. Chem. Soc. Faraday Trans. 2 85 (1989) 955.
[41] D.E. Stogryn, A.P. Stogryn, Mol. Phys. 11 (1966) 371.
[42] (a) M.L. Dubernet, J.M. Hutson, J. Chem. Phys. 98 (1994) 5844; (b) M.L. Dubernet, J.M. Hutson, J. Chem. Phys. 103 (1994) 1939.